GEOLOGICA CARPATHICA, 50, 3, BRATISLAVA, JUNE 1999
215–227

QUARTZ-APATITE-REE VEIN MINERALIZATION IN EARLY PALEOZOIC ROCKS OF THE GEMERIC SUPERUNIT, SLOVAKIA

IGOR ROJKOVIČ[1], PATRIK KONEČNÝ[2], LADISLAV NOVOTNÝ[3], ĽUBICA PUŠKELOVÁ[4] and VLADIMÍR STREŠKO[1]

[1] Faculty of Natural Sciences, Comenius University, Mlynská dolina, 842 15 Bratislava, Slovak Republic; rojkovic@fns.uniba.sk
[2] Geological Survey, Mlynská dolina 1, 817 04 Bratislava, Slovak Republic
[3] URANPRES, Fraňa Kráľa 2, 052 80 Spišská Nová Ves, Slovak Republic
[4] Geological Institute, Slovak Academy of Sciences, Dúbravská cesta 9, 842 26 Bratislava, Slovak Republic

(Manuscript received June 10, 1998; accepted in revised form March 17, 1999)

Abstract: Vein rare earth elements (REE) mineralization occurs in Early Paleozoic rocks of the Gemeric Superunit. Quartz-apatite veins near Čučma village contain a significant concentration of xenotime-(Y) accompanied by monazite-(Ce), allanite-(Ce), goyazite, and plumbogummite. Less significant accumulation of disseminated xenotime and its veinlets is also known near Betliar, Helcmanovce and Kociha villages. Near Kociha crandallite (?) was also found with increased contents of REE. The REE mineralization is accompanied by apatite, uraninite, brannerite, autunite, torbernite, quartz, pyrite, turmaline, rutile, titanite, marcasite and goethite. The content of REE and Y reaches up to several tenths of one weight percent and rarely even more than 1 weight percent in veins near Čučma. The other occurrences show only moderately increased contents of REE and Y (from 0.1 to 0.8 weight percent). Phosphates associated with metamorphosed black sediments are considered to be a source of the REE mineralization.

Key words: Gemeric Superunit, distribution of REE in minerals and rocks, REE minerals, veins.

Introduction

Quartz and quartz-apatite veins with uranium mineralization accompanied by rare earth element minerals have been found in the Early Paleozoic rocks of the Gemeric Superunit by the former Uranium Survey (Fig. 1). The veins are often situated in the vicinity of Gemeric granites. The uranium mineralization was found in the quartz veins accompanied by apatite and increased contents of REE near Čučma village (Šváb et al. 1966; Tréger 1973). This association became an object of mineralogical studies by Pelymsky (1967 in Tréger 1973), Melnikova (1973), Varček (1975, 1977) and Rojkovič (1993). Quartz, apatite, xenotime, uraninite, pyrite and molybdenite were found in quartz-apatite veins (Pelymskij 1967 in Tréger 1973). Monazite was identified later as well as a younger generation represented by younger quartz, siderite, Fe-dolomite, dolomite, pyrite, arsenopyrite, pyrrhotite, marcasite, tetrahedrite, chalcopyrite, sphalerite, jamesonite, etc. (Varček 1977). The younger stibnite mineralization in the area of Čučma and Betliar is represented by stibnite, chalcostibite, bournonite, boulangerite, berthierite, jamesonite, antimony, accompanied by pyrite, arsenopyrite, quartz, siderite, Fe-dolomite, pyrrhotite, sphalerite, chalcopyrite, galena and other minerals (Beňka & Caňo 1992). Less increased contents of P, Y and REE were found near Betliar, Helcmanovce and Kociha villages (Tréger 1973). Evansite was determined as the main phosphorus-bearing mineral in Kociha locality according to chemical composition (in weight percent): 22.55 P_2O_5, 26.61 Al_2O_3, 13.66 SiO_2, 0.56 Fe_2O_3 and 0.39 CaO as well as according to differential thermal analysis (Tréger 1973). Xenotime-(Y) together with uraninite, brannerite, native gold and other minerals were found in the Zimná voda Valley near Prakovce (Rojkovič et al. 1997). An increased content of P_2O_5 was found in the black phyllite and lydite (Oružinský et al. 1989; Varček et al. 1989; Rojkovič et al. 1995). The aim of this study was to identify REE minerals and characterize the REE distribution in rocks.

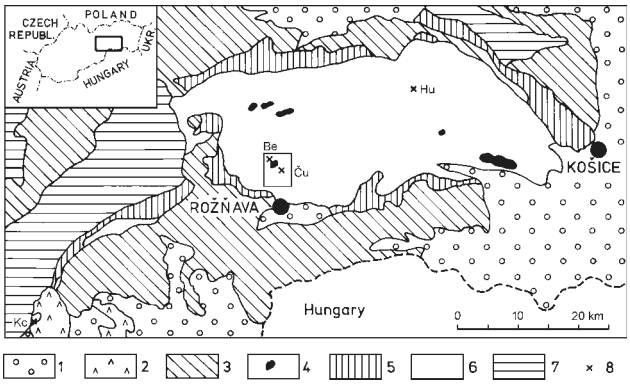

Fig. 1. Geological map of the eastern part of the Slovenské rudohorie Mts. (adapted according to Biely et al. 1996). 1 — Tertiary sediments, 2—Neogene volcanic rocks, 3—Mesozoic rocks, 4–6 — Gemeric Superunit, 4 — granite, 5 — Late Paleozoic rocks, 6 — Early Paleozoic rocks, 7 — Paleozoic and Proterozoic ? rocks of Veporic Unit, 8 — REE mineralization, Be — Betliar, Čučma — Čučma, Hu — Helcmanovce, Kc — Kociha. The frame in the centre represents the area of Fig. 2.

Methods

Minerals were studied by polarizing microscope in both transmitted and in reflected light and by scanning electron micro-

scope (SEM). They were analysed by wave-dispersion X-ray microanalysis (WDX), energy-dispersion X-ray microanalysis (EDX) and by X-ray diffraction analysis (XRD). Micropobe analyses were carried out on a JEOL-733 Superprobe X-ray microprobe equipped with KEVEX Delta IV+ energy dispersive system (Geological Survey of the Slovak Republic). Monazite and allanite were analysed with a JEOL-733 using 20 KV accelerating voltage, 20 nA beam current, 10 to 20 seconds counting times according to the total number of counts. The obtained counts were recalculated in oxides using PAP correction. Apatite, titanite were analysed with KEVEX ED system. The electron beam was stabilized on 1.2 nA with 15 KV accelerating voltage. Counts were acquired for 100 seconds and recalculated using XPP quantitative correction. The electron beam was focused on 3–5 micrometers. Natural and synthetic standards were applied to calibration of both systems: Al–Al_2O_3, Si–SiO_2, P–apatite, Ca–wollastonite, Fe–hematite, Y–YAl garnet, La–LaB_6, Ce–CeO_2, Pr–$PrPO_4$, NdSmYbLu–REE glass, Th–ThO_2, U–UO_2 and Cl–NaCl. Detection limits were better than 0.1 wt. %. Relative standard deviation ranged from ±5 % (for 1 wt. %) to ±25 % (for 0.1 wt %).

The chemical composition of the rocks was determined by chemical wet analysis and X-ray fluorescence analysis (XFA) for major elements of the rocks and by colorimetry for P_2O_5. Major elements were analysed on the X-ray spectrometer Philips PW 1410/20. Instrumental conditions: X-ray tube with Rh anode (voltage 40 kV, current 40 mA), gas flow detector with Ar/CH_4=90/10 filling, crystal LiF 200 for Fe, Mn, Ti, Ca, K and TlAP for Si, Al, Mg, Na. Samples (1.3 g) were fused with $Li_2B_4O_7$ (5.5 g) at the temperature of 1050 °C in Pt-crucible. The following standards were used: GM — granite, BM — basalt, TS — shale and their mixtures. Optical emission spectroscopy (OES) was used for trace elements (including La, Yb and Y in some samples). The spectra of samples were recorded by the grid spectrograph PGS-2 in UV and visual area, with 6 A power arch as the activating source. The measuring time was 90 s. Standard: GM — granite and TS — shale.

Rare earth elements were analysed by atomic emission spectroscopy with induction coupled plasma (AES-ICP). The decomposition procedure of samples by repeated treatment with acid mixture (HNO_3 + HF + $HClO_4$) and following fusion of the insoluble residue with $NaBO_2$ was used. REE were separated by catex ion exchanger DOWEX AG 500W-X8. Samples were analysed by sequential atomic emission spectrometer Plasmakon S 35. Detection limits ranged from 0.25 to 0.5 ppm. Relative standard deviation ranged from ±2 % (for 0.1 wt. %) to ±10 % (for 0.001 wt. %).

Geological setting and distribution of REE mineralization

Čučma

Quartz-apatite veins occur north of the village of Čučma in the Early Paleozoic rocks of the Bystrý Potok Formation (Bajaník et al. 1984). An adjacent rhyolite metatuff has been dated by U/Pb dating at 403 Ma (Cambel et al. 1990). The veins are accompanied by uranium mineralization and have increased contents of REE (Šváb et al. 1966; Tréger 1973). The most important mineralization is bound to a vein structure 1.7 km long (with segments of visible mineralization on the surface up to 25 m long), direction 60–70°, inclination 65° to SSE and average thickness of 0.6 m (maximum up to 3 m). It occurs 200 m north of a quartz vein with antimony mineralization exploited in the past in Gabriela adit and shaft (Fig. 2). Short quartz-apatite veins of direction 65°, inclination 35° to SE, length 50 m and thickness from 0.1 to 0.3 m occur also in rhyolite metatuff on the slopes of Majerská dolina Valley (Fig. 2). Sericite phyllite and metamorphosed black shale in Majerská dolina Valley contain lensoidal accumulations of apatite from 10 to 15 cm long (Šváb et al. 1966).

Quartz-apatite veins are accompanied by U-REE mineralization. Dominant quartz with apatite (up to more than 10 percent) are accompanied by xenotime, monazite, goyazite and plumbogummite (Fig. 3). Xenotime is the most important REE mineral of these veins reaching up to more than 1 percent, monazite ranges between 0.1 and 0.5 percent, goyazite less than 0.01 percent and rare plumbogummite was found in one sample only (Figs. 4, 5). The REE mineraliza-

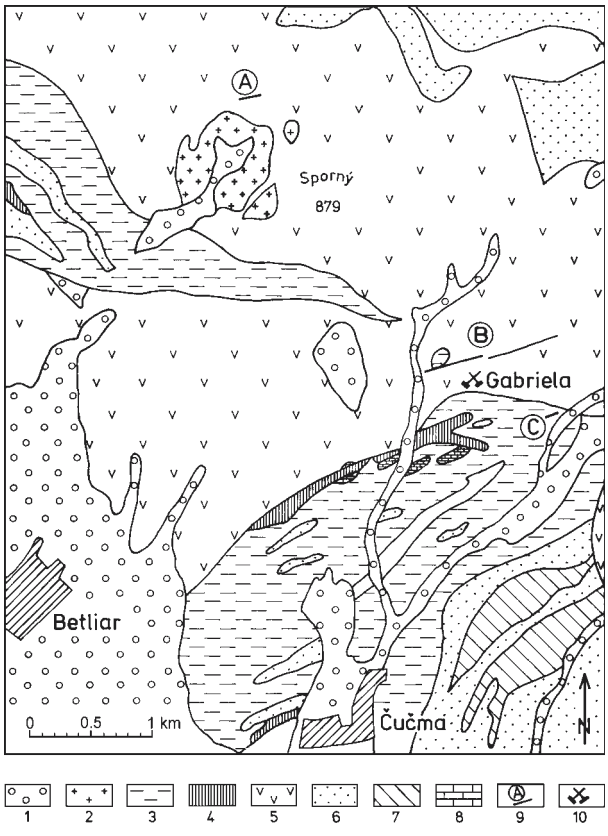

Fig. 2. Geological map of the Čučma and Betliar area (adapted according to Bajaník et al. 1984). 1 — Quaternary, 2 — granite, 3 — black phyllite, 4 — lydite, 5 — metarhyolite and its tuff, 6 — quartz phyllite and metamorphosed quartz wacke, 7 — chlorite-sericite phyllite, 8 — limestone, 9 — occurrences of REE mineralization, A — Betliar, B — Čučma vein north of Gabriela shaft, C — Majerská dolina Valley, 10 — mining dumps of abandoned antimony deposit Gabriela.

Fig. 3. Tabular crystals of apatite (white) in brown quartz (grey). Čučma,Ču 10.

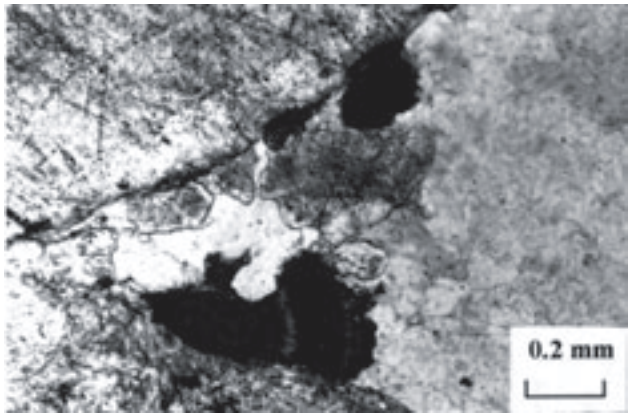

Fig. 4. Zonal xenotime (black) overgrows and in the form of thin veinlet cuts apatite (grey) in quartz (white). Čučma,Ču 5a, transmitted light, 1 nicol.

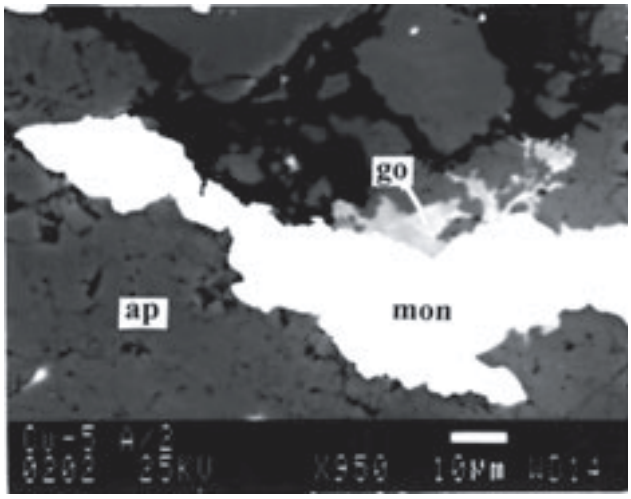

Fig. 5. Monazite veinlet (mon) cuts apatite (ap). Grains and veinlet of goyazite (go) occur at the contact of earlier minerals. Čučma,Ču 5a, SEM-BSE.

tion is accompanied by uraninite, brannerite, autunite, torbernite, apatite, quartz, pyrite, tourmaline and goethite. Besides the quartz-apatite veins the metatuff contains veinlets of quartz with disseminated allanite (around 0.5 percent) accompanied by xenotime and monazite (Fig. 6). The younger sulphide mineralization is associated with separated structures with dominant stibnite mineralization.

Regional rocks are represented by a rhyolite metatuff, granite, chlorite sericite phyllite, quartz-sericite phyllite, black phyllite and lydite. The metamorphosed rocks strike in E–W and NE–SW directions and dip 30–40° to the S or SE. The rhyolite metatuff is the wall rock of the veins. Sericitization is the typical wall rock alteration (Šváb et al. 1966). The Gemeric granite body was found by drilling underneath quartz-apatite vein in depth of 220 m (Šváb et al. 1966, Fig. 7). Frequent accessory minerals of the granite are tour-

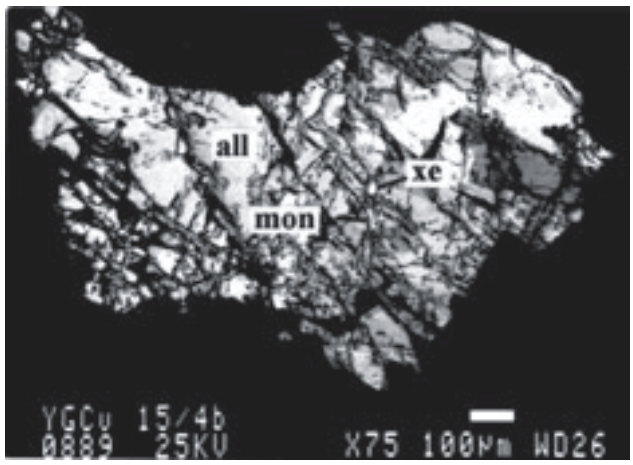

Fig. 6. Allanite aggregate of different brightness (all) reflecting a varying REE content with small grains and veinlets of xenotime (xe) and monazite (mon). Čučma,Ču 15/4, SEM-BSE.

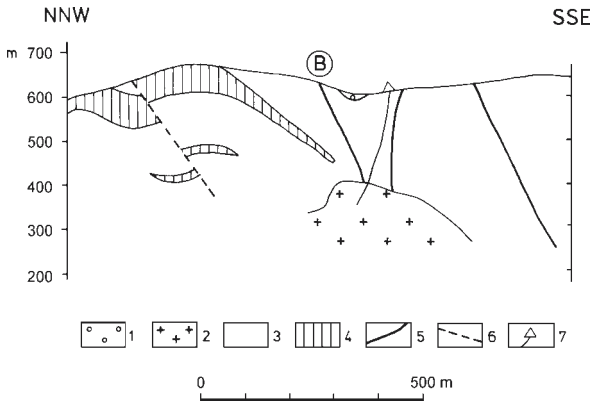

Fig. 7. Geological cross-section of quartz-apatite vein area near Čučma (adopted according to Šváb et al. 1966): 1 — Quaternary gravel, sand and clay, 2 — granite, 3 — metatuff of rhyolite and sericite phyllite, 4 — metarhyolite, 5 — vein, 6 — fault, 7 — drilling.

maline, apatite and pyrite (Gbelský 1982), which are also common minerals of the quartz-apatite veins.

Betliar

The REE mineralization occurs 6 km north of the village of Betliar in the mountain crest at an altitude of 755 m, 400 m SW of hill 806.4 (Fig. 2). Rhyolite metatuff with veinlets of quartz and iron hydroxides show increased radioactivity (up to 600 imp./s). the accumulation of apatite, rutile and titanite accompanied by rare xenotime and monazite is similar as that near Čučma but it is not so extensive and abundant (Fig. 8). The observed extent of mineralization is about 100 m with a direction of 80°, and inclination 50 to 60° towards the south and thickness from 0.2 to 1 m.

Helcmanovce

The occurrence is situated in the mountain crest (altitude 815 m), 300 m NW from Veľký hutný potok Stream and 2.6 km SW from the Helcmanovce village. U-REE mineralization is bound to a zone with veinlets of quartz and iron hydroxides showing E–W direction, length 200 m and thickness around 1 m as revealed by technical works of the former Uranium Survey. A mineralized tectonic zone contains accumulation of xenotime ranging from 0.5 to 1 percent (Fig. 9). Wall rock is represented by rhyolite metatuff and metarhyolite. It is accompanied by black phyllite, lydite, quartz-sericite phyllite, chlorite-sericite phyllite and small bodies of metabasalt and its metatuff. The rocks show an E–W direction of beds.

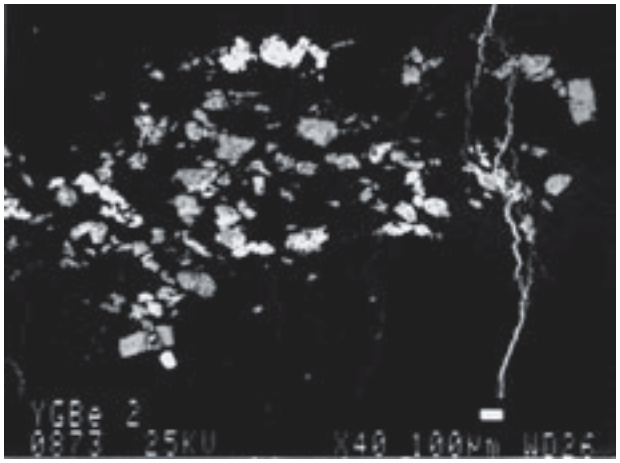

Fig. 8. Apatite crystals (grey) are accompanied by rutile (light grey) and titanite (detail in Fig. 19). They are cut by iron hydroxides (white). Betliar, Be 2, SEM-BSE.

Kociha

The abandoned adit of the former Uranium Survey is 1 km NE from the village of Kociha. The metamorphosed Early Paleozoic black sediments are the dominant rocks of the area. They are represented by black phyllite, lydite, carbonates and intercalations of rhyolite metatuff (Tréger 1973). They are covered by andesite tuff towards the east (Fig. 1). The shearing zone has a NE–SW direction and inclination from 60 to 80° towards the SE. It is intensively oxidized close to the surface and shows increased contents of P and REE. Quartz and quartz-carbonate veinlets several cm thick are bound to the shearing zone (up to 1.5 m thick) and they are accompanied by REE mineralization. Quartz-carbonate veinlets are accompanied by pyrite, marcasite, apatite, xenotime and crandallite (?) (Fig. 10). The wall rock is represented by *lydite* and limestone of the Early Paleozoic Gelnica Group.

REE and accompanying minerals

Apatite $Ca_5[(F,OH)|(PO_4)_3]$ occurs as tabular crystals from 0.05 mm to 1 cm long with longitudinal cleavage forming bands several millimetres thick (Fig. 3). It is accompanied by close association of quartz and pyrite. It is rimmed and enclosed by pyrite (Fig. 10). It is overgrown and cut by sericite, quartz, xenotime, monazite and uraninite (Figs. 4, 5, 11).

Xenotime $Y[PO_4]$ shows high relief, a brownish tint and distinct longitudinal cleavage (210) in transmitted light. It

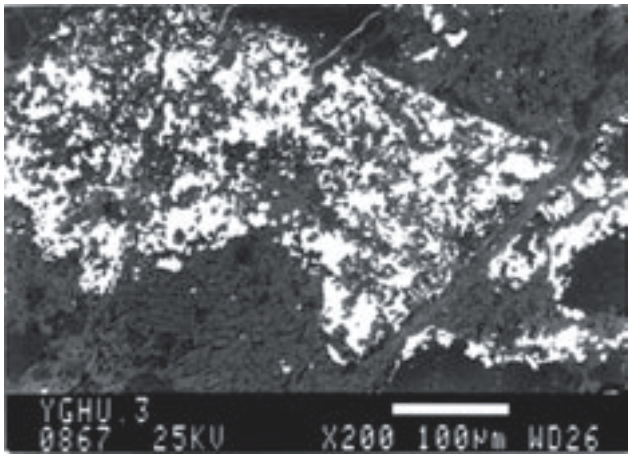

Fig. 9. Aggregate of xenotime (white) in rhyolite metatuff with abundant iron hydroxides (grey). Helcmanovce, Hu 3, SEM-BSE.

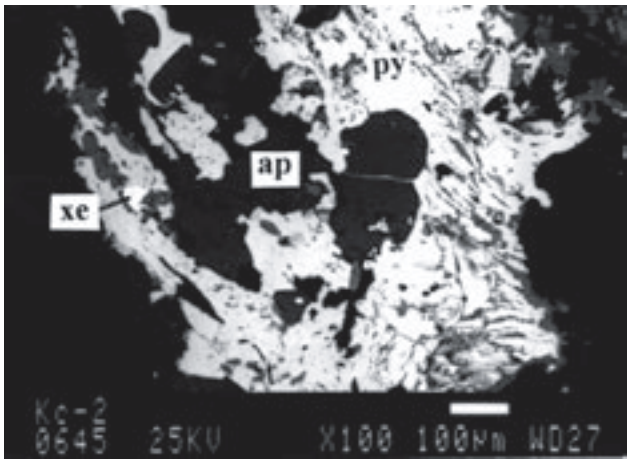

Fig. 10. Pyrite veinlet (py) enclosing apatite (ap) and xenotime (xe). Kociha, Kc 2, SEM-BSE.

forms radial, zonal or irregular aggregates (0.2 mm rarely up to 0.7 mm across) and clusters (rarely up to 1 mm across, Fig. 9). Fan-like aggregates overgrow apatite and fill the interstitial space of apatite grains (Fig. 4). The brown colour of aggregates due to intergrowing with goethite covers sometimes even vivid colours in crossed nicols. The radial aggregates often show cross zoning heightened by different tints of brown colour due to enclosures of uraninite, autunite and goethite. Xenotime crystals (up to 0.2 mm across) can be seen in quartz as well as in thin quartz veinlets cutting apatite. Small crystals from several μm up to 40 μm are enclosed in apatite, especially in its border and along fissures in apatite. The distinct zoning reflecting different uranium contents in xenotime can be observed in SEM (Fig. 12). Xenotime grains (from 50 to 150 μm across) were rarely found in pyrite-apatite veinlets as well as in colloform zonal aggregates of crandallite (?). Xenotime forms thin veinlets in apatite (Fig. 11). The chemical composition of xenotime shows the presence of uranium and HREE (Sm-Yb) as well as the main elements (Y a P) (Table 1, Fig. 13).

Monazite $Ce[PO_4]$ accompanies xenotime in veinlets and also forms separate veinlets in apatite (Fig. 5) and quartz (Fig. 14). Monazite grains vary in size from 10 μm to 0.2 mm across. Light rare earth elements (LREE) from La to Gd with dominant Ce were confirmed in its chemical composition (Table 2, Fig. 13).

Allanite $(Ca, Ce)_2(Fe^{\cdot\cdot},Fe^{\cdot\cdot\cdot})Al_2[O|OH|SiO_4|Si_2O_7]$ forms elongated crystals (2 to 4 mm long) and their aggregates in quartz veinlets (Fig. 15). Some grains show distinct longitudinal cleavage. It is accompanied by small grains and veinlets of monazite and xenotime in the intergranular space of allanite. SEM, EDX and WDX confirm the variability of its chemical composition as well as significant ratio of LREE (Table 3, Fig. 13). Different REE content is displayed even by back-scattered electron image in SEM. Darker domains are accompanied along cracks by veinlets and grains of monazite suggesting their secondary origin (Fig. 6). Darker domains along cracks are explained as a result of oxidation (Petrík et al. 1995). Allanite with low uranium content is, however, accompanied by secondary uranium minerals autunite and torbernite. Epidote was also found in some quartz veinlets.

Goyazite $SrAl_3H[(OH)_6(PO_4)_2]$ is a common minor mineral of the veins near Čučma (Rojkovič 1993). Small grains (up to 30 μm) or several μm thick veinlets fill fissures and interstitial space of apatite mainly close to monazite (Figs. 5, 16). It also occurs rarely in fissures of monazite. It was identified only by the help of WDX analysis on the basis of dominant Sr proportion partly replaced by LREE (Table 4, Figs. 13, 17).

Plumbogummite $PbAl_3H[(OH)_6(PO_4)_2]$ was found only as a rare mineral in the veins near Čučma. Small grains (several μm across) intergrown with goyazite replace apatite. It was identified only by WDX and EDX analysis according to the dominant proportion of Pb (Table 4). However, it represents a transitional member of the crandallite-goyazite series with significant proportion of Ca and minor proportion of Sr (Fig. 17).

Crandallite (?) $CaAl_3H[(OH)_6(PO_4)_2]$ was found in Kociha locality. Accumulation of iron hydroxides is accompanied by yellowish-white coloured fine-grained hydrous phosphates.

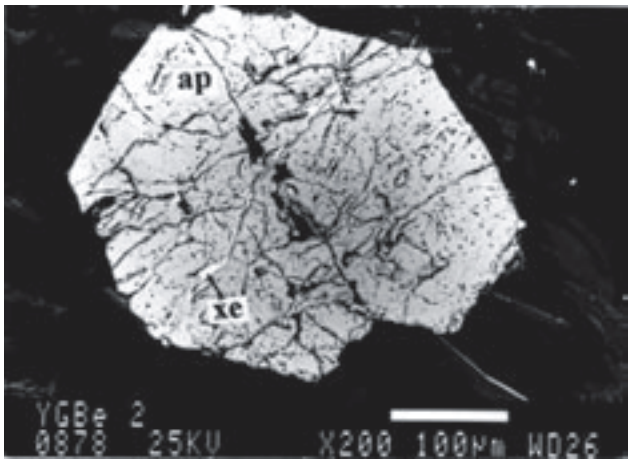

Fig. 11. Grains and veinlet of xenotime (xe) fill fissure of apatite (ap). Betliar, Be 2, SEM-BSE.

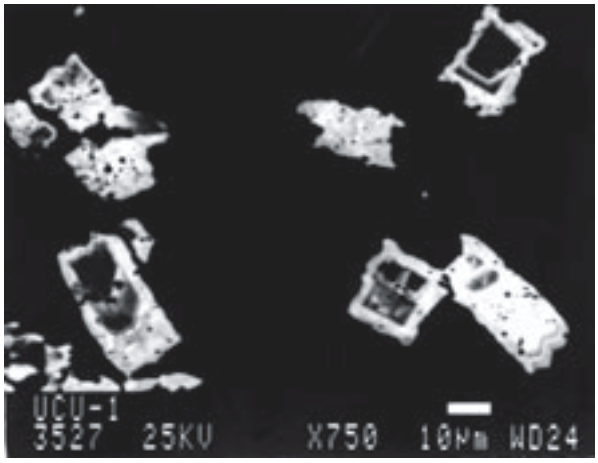

Fig. 12. Zonality of xenotime crystals due to different proportion of uranium (light zones are uranium-bearing). Čučma, Ču 1, back-scattered electron image (SEM-BSE).

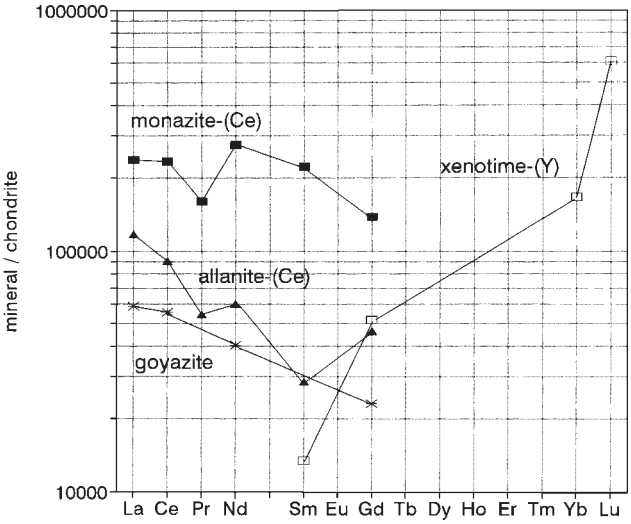

Fig. 13. Average REE distribution in the studied minerals.

Table 1: Chemical composition of xenotime.

	Weight percent														
Sample	Y_2O_3	Nd_2O_3	Sm_2O_3	Gd_2O_3	Tb_2O_3	Dy_2O_3	Ho_2O_3	Er_2O_3	Tm_2O_3	Yb_2O_3	Lu_2O_3	UO_2	HfO_2	P_2O_5	Total
Be 2.1	41.4	0.4	0.7	0.0	1.5	6.5	1.4	4.2	1.3	2.1	3.1	0.0	1.1	36.0	99.6
Be 2.2	37.8	0.0	0.0	2.3	1.5	6.5	1.4	4.2	1.3	4.5	0.2	0.1	0.0	40.4	100.1
Cu 1.1	43.4		1.0	4.3	1.6	7.3	0.0	2.5		5.1		1.6		32.8	99.7
Cu 1.2	47.0		0.8	3.7	0.0	6.4	0.0	2.7		4.7		1.4		33.0	99.7
Cu 1.3	49.4		0.8	2.4	0.0	4.0	0.0	2.3		6.0		1.0		33.9	99.9
Hu 3.2	43.8	0.4	0.5	0.0	1.3	5.4	1.8	4.2	1.6	1.5	1.8	0.0	0.9	34.6	97.8
Hu 3.3	43.4	0.2	0.3	0.0	1.3	5.4	1.8	4.2	1.6	2.6	2.6	0.0	1.0	32.2	96.6
Hu 3.4	40.1	0.0	0.0	1.7	1.3	5.4	1.8	4.2	1.6	4.5	2.1	0.0	0.0	37.5	100.1
Hu 3.6	39.3	0.0	0.0	2.4	1.6	5.7	1.4	4.3	1.4	3.2	2.3	0.0	0.0	38.5	100.1
Hu 3.7	40.5	0.4	0.6	0.0	1.2	6.1	0.0	4.9	1.5	3.0	3.2	0.0	0.8	36.6	98.7
Hu 3.8	37.5	0.0	0.0	2.4	1.2	6.1	0.0	4.9	1.5	6.1	3.4	0.0	0.0	36.9	100.0
Hu 3.9	40.5	0.2	0.8	0.0	1.2	6.0	1.9	4.8	1.9	2.9	3.4	0.0	1.0	34.1	98.7
Hu 3.10	37.5	0.0	0.0	1.9	1.2	6.0	1.9	4.8	1.9	5.5	2.7	0.0	0.0	36.8	100.0
Hu 3.11	35.8	0.0	0.0	1.8	1.2	6.2	1.9	5.3	2.2	5.4	2.7	0.0	0.0	37.3	99.9
Hu 3.12	43.8	0.6	0.9	0.2	1.5	5.8	1.4	3.8	1.7	1.5	2.2	0.0	0.5	38.7	102.4
Hu 3.13	42.8	0.0	0.0	2.8	1.5	5.8	1.4	3.8	1.7	3.6	1.8	0.0	0.0	35.1	100.1
Kc. 8.	36.8	0.0	0.0	3.6	1.7	6.2	1.9	3.7	1.5	4.9	0.0	0.1	0.0	39.7	100.1
Kc 95.1	36.3	0.0	0.0	3.8	1.6	5.7	1.8	3.7	1.9	4.9	0.6	0.1	0.0	39.7	100.1
Kc 95.2	36.2	0.0	0.0	3.7	1.6	6.1	2.0	3.5	1.6	5.0	1.2	0.1	0.0	39.3	100.1
Kc 95.6	45.6	0.0	0.0	3.8	0.0	6.2	0.0	4.7	0.8	3.7	1.1	0.0	0.0	34.3	100.2
Kc 95.7	42.1	0.0	0.0	4.9	0.0	6.9	0.0	5.1	0.9	5.1	1.5	0.0	0.0	33.6	100.1
Kc 95.8	38.2	0.0	0.0	4.7	0.0	6.8	0.0	4.9	2.0	4.8	1.8	0.0	0.0	37.0	100.1
	Atomic proportion on 4 oxygens														
	Y	Nd	Sm	Gd	Tb	Dy	Ho	Er	Tm	Yb	Lu	U	Hf	P	Total
Be 2.1	0.736	0.004	0.008	0.000	0.016	0.069	0.015	0.044	0.014	0.021	0.031	0.000	0.010	1.017	1.985
Be 2.2	0.638	0.000	0.000	0.024	0.015	0.066	0.014	0.042	0.013	0.044	0.002	0.001	0.000	1.084	1.944
Cu 1.1	0.794		0.012	0.049	0.018	0.081	0.000	0.027		0.054		0.012		0.953	2.000
Cu 1.2	0.846		0.010	0.041	0.000	0.070	0.000	0.029		0.048		0.010		0.945	2.000
Cu 1.3	0.874		0.009	0.027	0.000	0.043	0.000	0.024		0.061		0.008		0.954	2.000
Hu 3.2	0.794	0.005	0.006	0.000	0.015	0.059	0.020	0.045	0.017	0.015	0.019	0.000	0.009	0.997	1.999
Hu 3.3	0.819	0.003	0.004	0.000	0.015	0.061	0.020	0.047	0.018	0.028	0.028	0.000	0.010	0.966	2.019
Hu 3.4	0.700	0.000	0.000	0.018	0.014	0.057	0.019	0.043	0.016	0.045	0.020	0.000	0.000	1.041	1.973
Hu 3.6	0.677	0.000	0.000	0.026	0.017	0.060	0.014	0.044	0.014	0.032	0.022	0.000	0.000	1.057	1.962
Hu 3.7	0.717	0.005	0.007	0.000	0.013	0.066	0.000	0.052	0.016	0.031	0.032	0.000	0.007	1.032	1.976
Hu 3.8	0.665	0.000	0.000	0.027	0.013	0.066	0.000	0.052	0.016	0.062	0.034	0.000	0.000	1.040	1.973
Hu 3.9	0.744	0.003	0.009	0.000	0.014	0.066	0.021	0.052	0.020	0.031	0.035	0.000	0.010	0.995	2.000
Hu 3.10	0.665	0.000	0.000	0.021	0.013	0.064	0.020	0.050	0.019	0.056	0.027	0.000	0.000	1.039	1.974
Hu 3.11	0.634	0.000	0.000	0.019	0.013	0.066	0.020	0.056	0.023	0.055	0.027	0.000	0.000	1.051	1.966
Hu 3.12	0.737	0.006	0.010	0.002	0.015	0.060	0.014	0.038	0.017	0.015	0.021	0.000	0.004	1.036	1.974
Hu 3.13	0.765	0.000	0.000	0.031	0.016	0.063	0.014	0.040	0.018	0.036	0.018	0.000	0.000	0.999	2.001
Kc. 8.	0.628	0.000	0.000	0.038	0.018	0.064	0.019	0.037	0.015	0.048	0.000	0.001	0.000	1.079	1.947
Kc 95.1	0.620	0.000	0.000	0.040	0.017	0.059	0.018	0.037	0.019	0.048	0.006	0.001	0.000	1.080	1.946
Kc 95.2	0.622	0.000	0.000	0.040	0.017	0.063	0.021	0.036	0.016	0.049	0.011	0.001	0.000	1.075	1.950
Kc 95.6	0.817	0.000	0.000	0.043	0.000	0.067	0.000	0.050	0.009	0.038	0.012	0.000	0.000	0.979	2.014
Kc 95.7	0.771	0.000	0.000	0.056	0.000	0.076	0.000	0.055	0.010	0.054	0.016	0.000	0.000	0.977	2.015
Kc 95.8	0.674	0.000	0.000	0.051	0.000	0.073	0.000	0.051	0.020	0.049	0.018	0.000	0.000	1.038	1.974

They form colloform zonal aggregates mostly from 10 to 50 μm across (Fig. 18). They can be distinguished only by SEM. A high proportion of H_2O and variability of chemical composition in thin zones of colloform aggregates cause deviations from the formula of crandallite and a lower total in chemical composition by WDX analysis (Table 4). However the stable presence of Ca excludes evansite in the analysed material. It contains increased contents of Sr, LREE (La-Sm), Fe and Ba.

Uraninite UO_2 forms colloform zonal aggregates (up to 2 mm across) in quartz. Smaller grains and spheroids (from 1 to 3 μm across) are abundant in xenotime. They often form thin zones or bands several μm thick in xenotime. Uraninite shows significant lead contents from 1.5 to 1.8 weight percent).

Brannerite UTi_2O_6 or $(U,Ca,Th,Y)[(Ti,Fe)_2O_6]$ is a rare mineral of vein mineralization. Laths and rhombic sections of brannerite from 15 to 50 μm across were observed in the quartz of quartz-apatite veins. The chemical composition of brannerite corresponds to the formula $(U,Ca)_{0.99\text{-}1.07}(Ti,Fe)_{1.99\text{-}2.05}$, where, besides the main elements (U and Ti), low contents of Fe (up to 2.8 weight percent) and Ca (up to 1 weight percent) were observed.

Autunite $Ca[UO_2|PO_4]_2.10H_2O$ forms tabular crystals (from 0.1 to 0.5 mm across) and aggregates (up to 1.5 mm across) with distinct cleavage and vivid colours in crossed nicols in transmitted light. It fills fissures in vein minerals especially close to apatite. It overgrows apatite and intergrows with goethite. Its identification was confirmed by EDX analysis.

Torbernite $Cu[UO_2|PO_4]_2.10(12\text{-}8)H_2O$ forms aggregates of tabular crystals up to 0.5 mm in quartz. Lamellae of green colour form aggregates up to 1 mm across. Torbernite occurs in close association with goethite. Its chemical composition was confirmed by EDX analysis (Rojkovič 1997).

Pyrite FeS_2 occurs as irregular grains as well as euhedral crystals (pentagonal dodecahedrons and hexahedrons) from 5 μm to 0.5 mm across (mostly around 0.1 mm). Their aggregates usually reach around 2 mm across.

Rutile TiO_2 forms columnar crystals from 0.03 to 0.07 mm long and their clusters (up to 0.5 mm across). It accompanies

Table 2: Chemical composition of monazite.

	Weight percent												
Sample	**La_2O_3**	**Ce_2O_3**	**Pr_2O_3**	**Nd_2O_3**	**Sm_2O_3**	**Gd_2O_3**	**ThO_2**	**UO_2**	**CaO**	**FeO**	**Y_2O_3**	**P_2O_5**	**Total**
Cu5.1	9.6	25.9	2.2	19.2	5.3	4.9	0.0	0.2	0.3	0.0	0.7	30.1	98.4
Cu5.2	8.9	26.2	2.2	19.2	4.8	4.7	0.0	0.2	0.2	0.0	0.5	29.5	96.4
Cu5.3	8.4	25.6	2.3	19.4	5.4	5.2	0.2	0.3	0.3	1.0	0.7	30.4	99.2
	Atomic proportion on 4 oxygens												
Sample	**La**	**Ce**	**Pr**	**Nd**	**Sm**	**Gd**	**Th**	**U**	**Ca**	**Fe**	**Y**	**P**	**Total**
Cu5.1	0.140	0.376	0.032	0.272	0.073	0.064	0.000	0.002	0.012	0.000	0.014	1.011	1.996
Cu5.2	0.133	0.389	0.032	0.278	0.067	0.063	0.000	0.002	0.010	0.000	0.012	1.011	1.996
Cu5.3	0.121	0.367	0.033	0.272	0.074	0.068	0.001	0.003	0.011	0.034	0.014	1.010	2.007

Table 3: Chemical composition of allanite.

	Weight percent														
Sample	**Al_2O_3**	**SiO_2**	**P_2O_5**	**CaO**	**FeO**	**Y_2O_3**	**La_2O_3**	**Ce_2O_3**	**Pr_2O_3**	**Nd_2O_3**	**Sm_2O_3**	**Gd_2O_3**	**ThO_2**	**UO_2**	**Total**
Cu15.1	21.2	34.5	0.0	11.5	9.2	0.3	3.9	8.0	0.8	3.8	0.7	1.5	0.0	0.0	95.5
Cu15.2	19.9	32.9	0.1	12.9	9.9	0.0	4.9	9.4	0.7	3.5	0.5	1.3	0.0	0.0	96.1
Cu15.3	20.3	35.3	0.1	13.7	9.3	0.0	5.0	10.0	0.7	3.7	0.5	1.6	0.0	0.0	100.3
Cu15.4	20.5	34.9	0.1	9.5	8.9	0.0	4.7	10.4	0.9	4.4	0.5	1.4	0.0	0.1	96.2
Cu15.5	21.1	31.9	0.1	16.2	8.9	0.3	4.7	9.9	0.6	3.9	0.8	1.4	0.1	0.0	100.0
Cu12.1	19.2	33.1	0.1	10.6	12.1	0.3	3.0	10.3	0.8	5.1	0.8	2.0	0.0	0.1	97.5
Cu12.2	18.3	30.4	0.1	12.0	13.0	0.3	4.3	10.7	0.7	4.5	0.7	2.0	0.0	0.0	97.0
Cu12.3	18.5	32.1	0.1	9.1	12.9	0.0	4.6	11.3	0.7	4.8	0.8	2.1	0.0	0.0	97.1
	Atomic proportion on 12 oxygens														
Sample	**Al**	**Si**	**P**	**Ca**	**Fe**	**Y**	**La**	**Ce**	**Pr**	**Nd**	**Sm**	**Gd**	**Th**	**U**	**Total**
Cu15.1	2.190	3.020	0.003	1.080	0.673	0.016	0.126	0.257	0.026	0.118	0.021	0.044	0.001	0.000	7.575
Cu15.2	2.090	2.942	0.007	1.233	0.740	0.002	0.161	0.309	0.024	0.111	0.016	0.038	0.000	0.000	7.672
Cu15.3	2.038	3.009	0.007	1.250	0.661	0.000	0.158	0.311	0.022	0.112	0.016	0.045	0.000	0.000	7.629
Cu15.4	2.130	3.085	0.005	0.896	0.654	0.001	0.152	0.335	0.029	0.140	0.014	0.042	0.000	0.002	7.484
Cu15.5	2.159	2.775	0.010	1.507	0.644	0.012	0.152	0.315	0.020	0.121	0.025	0.042	0.002	0.000	7.784
Cu12.1	2.027	2.962	0.010	1.014	0.909	0.016	0.100	0.337	0.026	0.161	0.023	0.058	0.000	0.002	7.646
Cu12.2	1.994	2.811	0.007	1.191	1.007	0.016	0.147	0.363	0.025	0.149	0.022	0.061	0.000	0.000	7.791
Cu12.3	2.000	2.940	0.011	0.896	0.991	0.000	0.157	0.380	0.024	0.156	0.025	0.063	0.000	0.000	7.642

Table 4: Chemical composition of crandallite series minerals.

	Weight percent												
Sample *	**Al_2O_3**	**P_2O_5**	**CaO**	**SrO**	**La_2O_3**	**Ce_2O_3**	**Pr_2O_3**	**Nd_2O_3**	**Sm_2O_3**	**Gd_2O_3**	**PbO**	**Fe_2O_3**	**BaO**	**Total**
Cu 1.1 go	30.8	28.2	0.4	11.9	2.0	5.6	0.0	2.5	0.0	0.6	0.0	0.1	0.0	82.1
Cu 1.2 go	30.2	28.9	0.7	9.4	1.4	5.9	0.0	3.8	0.0	1.3	1.4	3.9	0.0	86.9
Cu 1.3 pg	27.8	26.8	2.4	2.6	1.2	3.3	0.0	2.2	0.0	0.0	14.0	3.9	0.0	84.2
Cu 5.1 go	33.2	26.4	0.9	11.5	2.4	6.5	0.0	2.7	0.0	0.7	0.4	0.9	0.0	85.6
Cu 5.2 go	29.3	24.1	1.0	9.9	3.0	6.5	0.0	2.3	0.0	0.7	0.2	4.2	0.0	81.2
Kc 95.1 cd	31.9	22.0	8.2	2.0	0.0	0.1	0.2	0.6	0.0	0.0	0.0	2.9	0.5	68.3
Kc 95.2 cd	31.9	25.4	9.5	1.3	0.0	0.0	0.3	0.3	0.0	0.0	0.0	2.6	0.3	71.5
Kc 95.3 cd	32.2	25.8	9.5	1.9	0.0	0.0	0.6	0.5	0.1	0.0	0.0	2.3	0.8	73.5
Kc 95.4 cd	31.3	24.9	8.3	1.6	0.0	0.0	0.3	0.6	0.4	0.0	0.0	2.6	0.5	70.4
Kc 95.5 cd	30.7	20.6	7.4	1.9	0.0	0.9	0.6	1.1	0.0	0.0	0.0	3.0	1.3	67.6
Kc 95.6 cd	31.1	24.4	8.5	2.0	0.2	0.3	0.4	0.7	0.2	0.0	0.0	3.4	0.7	71.9
Kc 95.7 cd	30.7	26.6	7.5	1.7	0.2	0.9	0.4	0.6	0.1	0.0	0.0	2.9	0.7	72.2
	Atomic proportion on 6 atoms													
Sample *	Al	P	Ca	Sr	La	Ce	Pr	Nd	Sm	Gd	Pb	Fe	Ba	Total
Cu 1.1 go	3.048	2.004	0.036	0.579	0.062	0.172	0.000	0.075	0.000	0.017	0.000	0.007	0.000	6.000
Cu 1.2 go	2.885	1.983	0.061	0.442	0.042	0.175	0.000	0.110	0.000	0.035	0.031	0.238	0.000	6.000
Cu 1.3 pg	2.863	1.982	0.225	0.132	0.039	0.106	0.000	0.069	0.000	0.000	0.329	0.256	0.000	6.000
Cu 5.1 go	3.157	1.804	0.078	0.538	0.071	0.192	0.000	0.078	0.000	0.019	0.009	0.055	0.000	6.000
Cu 5.2 go	2.981	1.761	0.093	0.496	0.096	0.205	0.000	0.071	0.000	0.020	0.005	0.273	0.000	6.000
Kc 95.1 cd	3.275	1.627	0.768	0.099	0.000	0.002	0.006	0.019	0.000	0.000	0.000	0.188	0.017	6.000
Kc 95.2 cd	3.121	1.785	0.845	0.060	0.000	0.000	0.008	0.010	0.000	0.000	0.000	0.161	0.010	6.000
Kc 95.3 cd	3.101	1.784	0.830	0.088	0.000	0.000	0.017	0.014	0.002	0.000	0.000	0.139	0.026	6.000
Kc 95.4 cd	3.144	1.800	0.761	0.078	0.000	0.000	0.010	0.017	0.010	0.000	0.000	0.164	0.016	6.000
Kc 95.5 cd	3.271	1.578	0.714	0.102	0.000	0.029	0.021	0.036	0.000	0.000	0.000	0.203	0.048	6.000
Kc 95.6 cd	3.097	1.746	0.766	0.096	0.007	0.010	0.012	0.021	0.006	0.000	0.000	0.216	0.023	6.000
Kc 95.7 cd	3.060	1.903	0.681	0.082	0.007	0.027	0.012	0.017	0.002	0.000	0.000	0.186	0.023	6.000

* cd — crandallite (?), go — goyazite, pg — plumbogummite

apatite near Betliar village (Fig. 19). WDX microanalysis confirmed Fe content up to 1.3 weight percent).

Titanite grains (up to 50 μm across) are closely associated and intergrown with rutile. It overgrows and encloses xenotime (Fig. 19).

Goethite α-FeOOH **and limonite** form aggregates up to 5 mm across filling fissures of apatite and quartz. It replaces pyrite and forms pseudomorphs after pyrite in quartz (up to 0.7 mm across). Thin zones of goethite accumulation were observed in xenotime aggregates. An increased content of uranium was found in some grains of goethite (up to 3.7 weight percent).

Quartz is brown with different grain size showing a mosaic structure and mostly direct extinction. A alternating layers with different grain size were observed. Mostly fine-grained

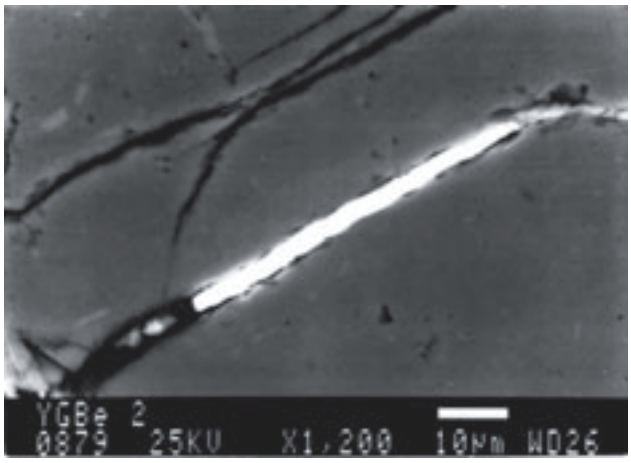

Fig. 14. Thin monazite veinlet in quartz. Betliar, Be 2, SEM-BSE.

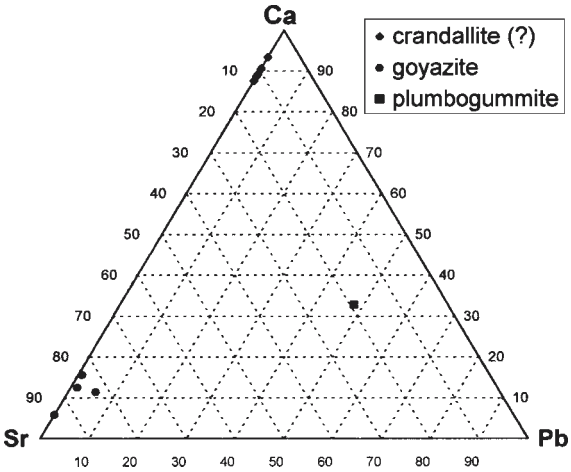

Fig. 17. Atomic proportion of Sr, Pb and Ca in crandallite series minerals (Čučma and Kociha localities).

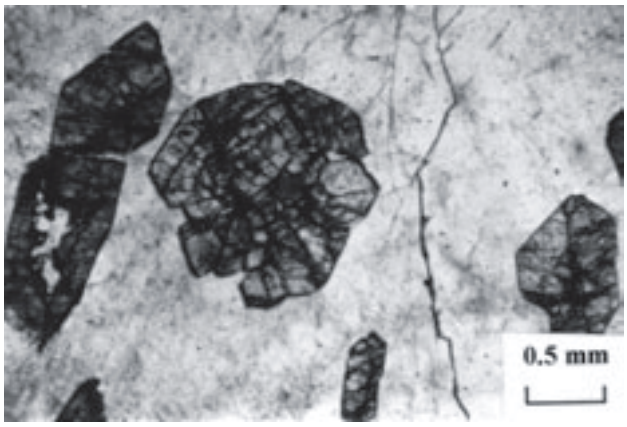

Fig. 15. Euhedral allanite (dark grey) in quartz. Čučma, Čučma 15/4, transmitted light, 1 nicol.

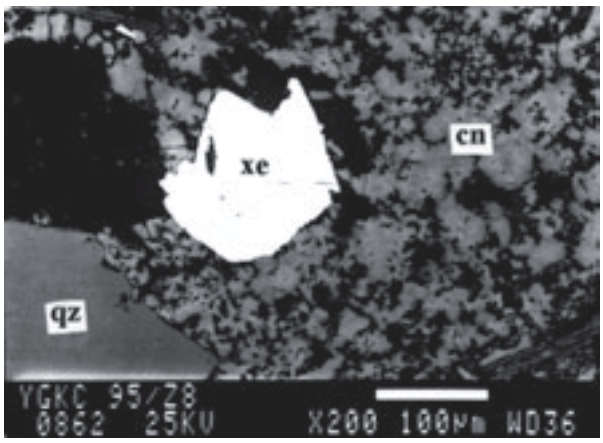

Fig. 18. Aggregate of crandallite (?) (cn) in quartz (qz) encloses xenotime (xe). Kociha, Kc 95/Z8, SEM-BSE.

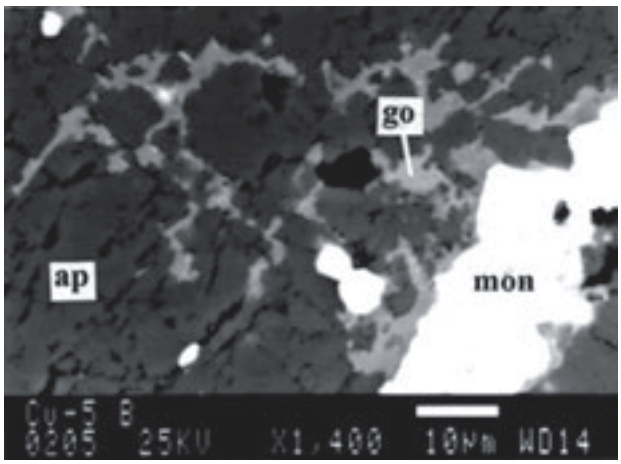

Fig. 16. Goyazite (go) replacing apatite (ap) along grain boundaries close to monazite veinlet (mon). Čučma, Čučma 5b, SEM-BSE.

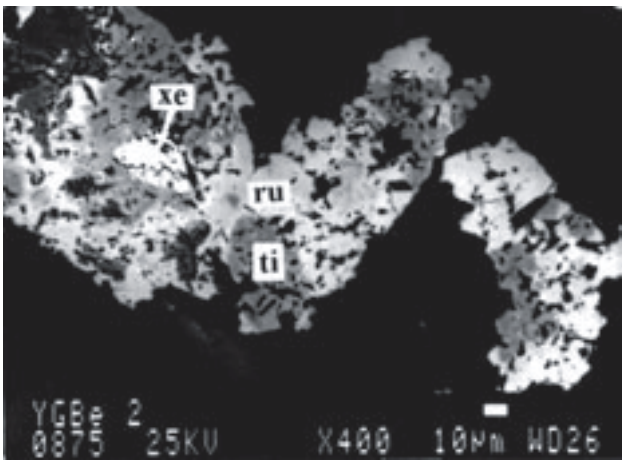

Fig. 19. Rutile (ru) intergrows with titanite (ti), enclosing xenotime (xe). Betliar, Be 2, SEM-BSE (detail of the upper part of Fig. 8).

zones are in contact with apatite. Veinlets of coarse-grained quartz (from 0.1 to 1 mm) cut carbonates and fine-grained quartz (0.01–0.2) with apatite and pyrite.

Carbonate grains (mostly from 1 to 2 mm across) forming mosaic structure are dominant only in Kociha locality in quartz-carbonate veinlets accompanied by pyrite, marcasite, apatite, xenotime and crandallite (?). They occur rarely in Čučma veins.

Sericite $KAl_2[(OH,F)_2\ AlSi_3O_{10}]$ lamellae (from 0.05 to 0.1 mm long) form aggregates (from 0.3 mm to several mm in size) rimming apatite. It also forms veinlets (up to 0.01 mm thick) in quartz.

Tourmaline $Na(Mg, Fe, Mn, Li, Al)_3Al_6(BO_3)_3(OH, F)_4[Si_6O_{18}]$ is abundant in some samples of the veins. Prismatic crystals with distinct pleochrosim (from 0.05 to 0.1 mm long) sometimes form bands parallel to zones of quartz with a different size of grains. It overgrows and rims apatite. It often intergrows with xenotime.

Geochemical characteristic

The contents of major and minor elements in rocks near the Čučma locality reflect their mineral composition. Metamorphosed shale-phyllite shows increased in the proportions of alumina (Table 5), organic carbon, Ba, Cr, Mo and V. The veins with studied mineralization show increased contents of Ca and P, reflecting abundant apatite. The trace elements of quartz and quartz-apatite veins are characterized by increased contents of U, Pb, Mo, Au, Y and La (Table 6). Increased contents of Co reflect abundant pyrite. The content of REE and Y in veins attain up to several tenths of weight percent and rarely even more than 1 weight percent (Table 7). The increased content of HREE reflects dominant xenotime in samples Cu 4a, 5a, 5b and 10 (Fig. 20).

The mineralized rhyolite metatuff near the Helcmanovce village is enriched in Y, HREE and uranium (Tables 6, 7). Increased content of Fe_2O_3 and loss of ignition (LOI) reflects the presence of iron hydroxides in sample with abundant xenotime (Hu 3, Table 5). The maximum content of Y 0.5 weight percent with REE content 0.3 weight percent reaches in total 0.8 weight percent. The distribution of REE in metatuff with xe-

Table 5: Chemical composition of rocks (in weight percent).

Sample	rock	SiO_2	TiO_2	AL_2O_3	Fe_2O_3	FeO	MnO	MgO	CaO	Na_2O	K_2O	P_2O_5	LOI	H_2O-	Total
Be 3	RT	69.49	0.45	15.11	1.64	0.05	0.010	1.11	2.04	0.18	4.10	2.31	2.96	0.36	99.81
Be 7	G	74.93	0.06	13.97	0.73	0.18	0.030	0.42	0.68	3.13	4.14	0.19	0.89	0.23	99.58
Be 8	G	71.99	0.15	15.10	1.06	0.32	0.020	0.72	0.55	3.30	4.90	0.23	1.17	0.19	99.58
Cu 10	Iqa	52.48	0.27	4.19	3.41	0.30	0.013	6.14	21.37	0.48	1.90	5.62	1.29	0.25	97.71
Cu 15.4	R	74.82	0.43	9.77	1.37	0.04	0.010	0.82	6.75	0.14	2.19	0.94	2.18	0.33	99.79
Cu 26.2	Iqa	86.06	0.05	4.11	0.73	0.43	0.014	0.20	3.45	0.41	1.15	2.42	0.71	0.15	99.88
Cu 27.2	Iq	92.25	0.04	2.07	2.07	0.48	0.013	0.07	0.07	0.38	0.58	0.06	1.37	0.13	99.88
Cu 30	RT	66.35	0.27	16.04	1.94	2.67	0.050	1.88	1.46	3.76	3.19	0.17	1.53	0.08	99.39
Cu 31	RT	67.10	0.27	16.54	1.00	3.35	0.050	1.55	1.75	3.37	3.01	0.21	1.21	0.20	99.61
Cu 32	Bc	42.53	0.31	30.79	3.16	5.00	0.070	3.11	0.16	0.90	7.55	0.17	5.59	0.22	99.56
Cu 33	Bcq	77.95	0.07	10.50	0.52	2.61	0.030	1.69	0.15	0.90	2.67	0.10	2.37	0.06	99.62
Cu 34	G	73.21	0.12	15.56	0.13	0.76	0.020	0.39	0.23	3.49	4.19	0.26	0.90	0.06	99.32
Cu 35	Bc	53.50	0.25	25.08	1.27	3.56	0.060	1.46	0.20	0.94	7.46	0.21	5.45	0.10	99.54
Hu 1	R	76.35	0.09	11.74	0.76	0.32	0.006	0.34	0.02	0.21	8.71	0.06	0.88	0.06	99.48
Hu 3	R	77.29	0.06	11.96	2.06	0.14	0.024	0.80	0.04	1.56	3.51	0.09	2.06	0.02	99.53
Kc 8	Iq	66.36	0.11	5.10	13.82	0.15	0.008	0.08	1.03	0.12	0.27	8.49	8.10	4.39	99.54
Kc 66	Bcq	86.03	0.19	3.46	0.42	0.04	0.002	0.23	0.03	0.11	0.87	0.05	8.09	0.07	99.54

Bc — black phyllite, Bcq — lydite, G — granite, Iq — quartz vein, Iqa — quartz-apatite vein, R — metarhyolite, RT — metatuff of rhyolite

Table 6: Trace elements in rocks (in ppm).

Sample	rock	Ag	Au	B	Ba	Co	Cr	Cu	La	Mo	Ni	Pb	Sr	Sn	Ti	U	V	W	Zr	Y
Be 2	RT	0.5		41	617	16.6		26	100	1.5	4.8	89.0	48.0	26.3	2900		69.0	79	204	71
Be 3	Iq	35.0		93	776	16.1		31	363	3.2	5.1	3700.0	55.0	36.3	3900		85.0	89	269	400
Be 5	RT	0.5		45	617	9.3		32	85	0.5	3.9	60.0	47.0	41.7	2950		78.0	58	177	83
Be 7	G	0.5		89	209	10.4		4	15	0.5	3.2	21.0	8.0	14.8	562		1.5	40	37	19
Be 8	G	0.5		89	437	6.9		3	15	0.5	3.8	10.0	15.0	20.4	1380		10.0	35	123	17
Cu 4 a	Iqa	1.2	0.0250		296	47.0	32		212		47.0					68				
Cu 4 b	Iqa	1.6	0.0090		995	8.0	40		160		51.0					173				
Cu 4 c	Iqa	1.3	0.2000			127.0	25		214		40.0					150				
Cu 10	Iqa	0.7		24	138	34.0		15	407	4.0	26.0	70.0	73.0	18.2	1180	370	27.0	6	49	6050
Cu 15.4	Iq	1.0		20	282	14.8		51	245	2.2	5.3	348.0	79.0	23.9	2700	1320	28.0	107	175	700
Cu 26.2	Iqa	2.1		101	260	28.0		16	165	279.0	17.0	103.0	73.0	19.3	463	1700	28.0	55	11	2487
Cu 27.2	Iq	0.7		42	70	182.0		27	18	2.8	62.0	52.0	5.0	2.0	381	49	6.0	72	29	20
Cu 30	RT	0.5	0.0170	59	485	49.0	96	20	101	20.0	21.0	32.0	19.0	6.4	1110	1	569.0		70	46
Cu 31	RT	0.5	0.0009	45	1430	36.0	36	21	39	2.4	21.0	65.0	157.0	8.2	3650	2	78.0	224	433	46
Cu 32	Bc	0.5	0.0020	152	1920	26.0	110	32	34	149.0	40.0	9.0	40.0	29.7	3270	24	284.0	21	55	40
Cu 33	Bc	0.5	0.0040	58	825	44.0	93	8	51	307.0	38.0	7.0	10.0	21.2	3100	3	377.0		189	31
Cu 34	G	0.5	0.0450	279	351	40.0	6	6	15	1.8	9.0	16.0	5.0	35.9	768	46	1.5	8	36	22
Cu 35	Bc	0.5	0.0008	130	2010	42.0	105	39	37	2.8	55.0	8.0	26.0	14.6	3400	4	230.0		90	53
Hu 1	R	0.5	0.0059	39	184	5.0	6	3	57	0.5	4.0	1.5	1.5	1.3	474	4	1.5		30	40
Hu 3	R	2.1	0.0005	46	196	10.0	1	123	40	0.5	16.0	74.0	1.5	15.6	381	1810	29.0	24	108	3100
Kc 1	Bcq	0.7	0.0150		950	26.0	82		34		53.0					45				
Kc 7	Iq	1.8	0.0004	28	1930	45.0	290	160	225	124.0	96.0	56.0	1100.0	8.9	2310	105	472.0	3	189	574
Kc 8	Iq	0.5	0.0083	15	1850	12.0	188	106	1100	216.0	20.0	700.0	1100.0	4.1	1240	87	272.0	16	97	871
Kc 31	Bcq	0.5	0.0003	40	948	10.0	61	16	126	1.5	8.0	13.0	9.0	0.5	1940	1	137.0	39	66	13
Kc 66	Bcq	0.5	0.0004	17	472	7.0	62	13	98	34.0	9.0	8.0	5.0	1.0	1880	3	460.0	30	74	75
Kc 84	Bcq	0.5	0.0001	11	399	12.0	31	12	174	23.0	6.0	5.0	8.0	0.5	980	2	332.0	61	34	47
Kc 95.1	Bcq	0.5		44	146	3.9	330	86	158	9.1	7.5	13.0	54.0	1.5	146		161.0		2	69

Bc — black phyllite, Bcq — lydite, G — granite, Iq — quartz vein, Iqa — quartz-apatite vein, R — metarhyolite, RT — metatuff of rhyolite

Table 7: Rare earth elements in rocks (in ppm).

Sample	rock	La	Ce	Pr	Nd	Sm	Eu	Gd	Tb	Dy	Ho	Er	Tm	Yb	Lu	Σ_{REE}	Y	Σ_{REE+Y}
Be 3.4	Iq	191.0	261.0	32.0	125.0	20.0	6.0	39.0	6.0	53.0	10.0	26.0	3.0	20.0	3.0	795.0	234.0	1029.0
Cu 4 a	Iqa	212.0	1050.0	12.0	750.0	291.0	44.0	315.0	56.0		58.5		21.8	126.0	15.4	2951.7		
Cu 4 b	Iqa	160.0	1130.0	91.0	1050.0	435.0	50.0	565.0	87.0		65.5		47.0	263.0	35.5	3979.0		
Cu 4 c	Iqa	214.0	1070.0	87.0	765.0	295.0	48.5	340.0	45.5		37.5		19.6	107.0	16.4	3045.5		
Cu 5 a	Iqa	515.0	1330.0	200.0	857.0	505.0	75.3	580.0	161.0	955.0	165.0	451.0	59.2	365.0	38.6	6257.1	4630.0	10887.1
Cu 5 b	Iqa	586.0	1430.0	205.0	963.0	547.0	66.4	639.0	148.0	1040.0	154.0	476.0	55.9	399.0	41.3	6750.6	5040.0	11790.6
Cu 10	Iqa	407.0	972.0	163.0	1038.0	341.0	73.0	709.0	162.0	1142.0	214.0	566.0	74.0	410.0	25.0	6296.0	6050.0	12346.0
Cu 14.3	Iqa	254.0	465.0	70.0	330.0	68.0	14.0	54.0	6.0	52.0	6.0	16.0	3.0	12.0	3.0	1353.0	153.0	1506.0
Cu 15.4	R	146.0	261.0	35.0	213.0	74.0	26.0	136.0	26.0	172.0	30.0	78.0	9.0	60.0	3.0	1269.0	696.0	1965.0
Cu 21.1	Iqa	116.0	244.0	39.0	244.0	74.0	35.0	62.0	7.0	38.0	3.0	11.0	3.0	7.0	3.0	886.0	114.0	1000.0
Cu 26.2	Iqa	165.0	379.0	60.0	410.0	152.0	43.0	324.0	75.0	526.0	96.0	254.0	33.0	193.0	12.0	2722.0	2487.0	5209.0
Cu 31	RT	43.5	90.4	10.7	40.2	9.0	1.3	7.5	1.0	6.4	1.2	2.6	0.4	2.9	0.4	217.5	30.7	248.2
Cu 32	Bc	50.4	114.0	12.9	45.1	9.9	1.8	7.8	1.2	5.6	1.1	1.9	0.4	2.9	0.4	255.4	26.0	281.4
Cu 34	G	5.4	10.7	3.0	5.1	1.3	0.9	3.2	0.2	2.2	0.5	1.0	0.3	1.3	0.2	35.4	14.2	49.6
Hu 1	R	25.7	50.4	7.1	28.5	8.1	0.4	8.1	1.2	9.0	1.8	3.0	0.6	5.5	0.5	149.9	46.7	196.6
Hu 3	R	11.1	40.8	9.5	50.1	95.1	4.0	330.0	82.5	735.0	163.0	283.0	46.4	288.0	34.5	2173.0	4530.0	6703.0
Hu 4	R	48.0	101.0	18.0	124.0	86.0	5.8	390.8	101.0	860.5	172.6	509.5	69.8	397.7	54.4	2939.1	5210.0	8149.1
Hu 5	R	38.0	86.0	12.0	111.0	80.0	5.0	341.8	82.0	657.9	127.7	369.3	50.4	289.0	40.0	2290.1	4071.0	6361.1
Hu 6	R	24.0	42.0	6.0	48.0	48.0	3.4	261.5	74.0	596.1	119.3	352.5	47.5	258.2	36.4	1916.9	3926.0	5842.9
Kc 1	Bcq	34.0	85.0	4.0	26.0	5.3	1.1	4.3	0.8		1.1		0.4	1.9	0.3	164.2		
Kc 8	Iq	495.0	990.0	103.9	438.0	130.9	24.9	140.0	15.9	93.8	17.0	26.2	3.9	37.7	3.3	2520.4	417.0	2937.4
Kc 66	Bcq	11.6	22.7	3.1	13.2	4.0	0.2	4.0	0.9	5.8	1.3	2.2	0.5	4.0	0.5	73.8	55.0	128.8

Bc — black phyllite, Bcq — lydite, G — granite, Iq — quartz vein, Iqa — quartz-apatite vein, R — metarhyolite, RT — metatuff of rhyolite

notime accumulation with dominant HREE is distinctly different from non-mineralized metatuff with dominant LREE (Fig. 21).

The chemical composition of the rhyolite metatuff with quartz veinlets near Betliar shows increased contents of CaO and P_2O_5 (over 2 weight percent) reflecting accumulation of apatite (Table 5). The content of REE and Y exceed 1000 ppm (Table 7). Chondrite normalized REE distribution patterns confirm increased LREE as well as HREE in sample Be 3.4 (Fig. 22). A mineralized sample with quartz veinlets near the Kociha village (sample Kc. 8) shows P_2O_5 content over 8 weight percent and Fe_2O_3 content over 13 weight percent reflecting abundant presence of iron hydroxides and crandallite (?) (Table 5). Crandallite (?) also increases the contents of LREE and Ba (Tables 2 and 3, Fig. 22). The transitional composition of crandallite-goyazite series is reflected in increased contents of Sr (Table 6). The increased con-

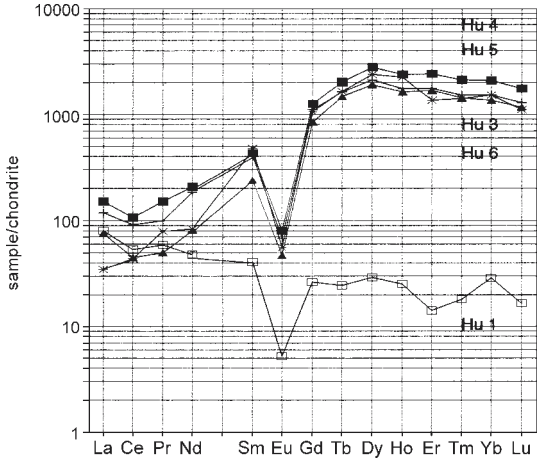

Fig. 21. Distribution of REE in rhyolite metatuff without (Hu 1) and with xenotime accumulation (Hu 3, 4, 5 a 6) near Helcmanovce.

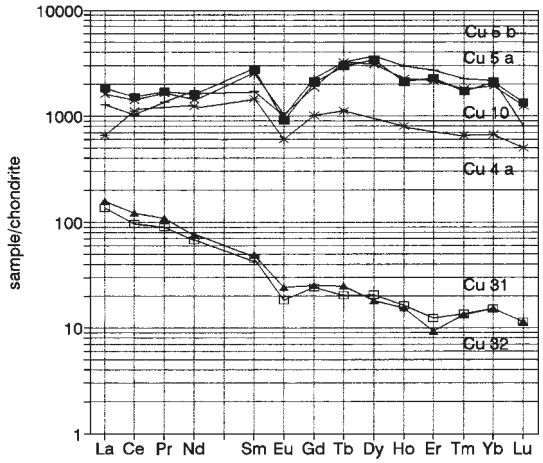

Fig. 20. Distribution of REE in quartz-apatite veins near Čučma (Cu-4, 5a, 5b a 10), in rhyolite metatuff (Cu 31) and in black phyllite (Cu 32).

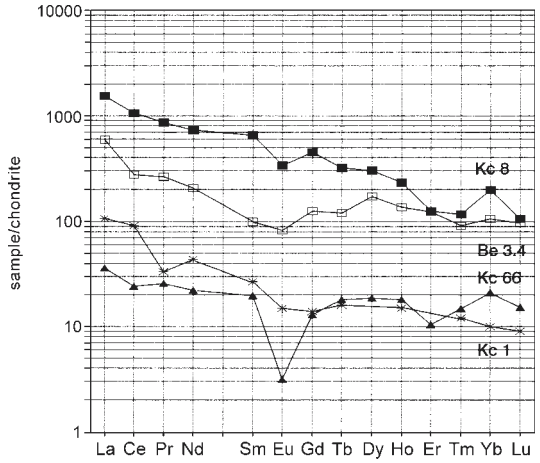

Fig. 22. Distribution of REE in mineralized metatuff of rhyolite near Betliar (Be 3.4 — open square), in lydite (Kc 1 — asterix and Kc 66 — full triangle) and in mineralized lydite (Kc 8 — full square) near Kociha.

tent of Y is related to the confirmed xenotime (Tables 6, 7). Maximal content of REE attains 2520 ppm and Y 417 ppm.

Discussion

The REE frequently accompany elements of uranium mineralization. REE, especially heavy rare earth elements (HREE) and Y, can substitute uranium in the uraninite structure (Pagel et al. 1987; Bea 1996). Part of xenotime can be formed by release and remobilization of Y and HREE from the structure of uraninite and brannerite and by reactions with mobile phosphates (Oberthür 1987; Rojkovič et al. 1997). There are numerous studies confirming the mobility of REE during metamorphism, hydrothermal alteration and the formation of shear zones. However, large fluid versus rock ratios are necessary to cause changes of REE distribution pattern during regional metamorphism of silicates. Retrograde shear zones characterized by abundant hydrous minerals appear to be extremely favourable for REE mobilization (Lottermoser 1992). The mobility of REE, especially that of HREE is often associated with uranium transport as carbonate complexes, uranyl fluoride complexes and uranyl phosphate complexes. Uranium and REE were transported mostly by carbonate complexes even in a low temperature, alkaline and oxidizing solution in the Pine Creek Geosyncline (McLennan & Taylor 1979). HREE are leached more easily in an environment close to neutral (pH from 6 to 7) and light rare earth elements (LREE) in a more acid environment (Shmaryovich et al. 1989). Easier mobility of Y and HREE is also suggested by rims of newly formed xenotime-(Y) rims around zircon in metamorphosed rocks (Vocke et al. 1987; Rojkovič et al. 1989). Hydrothermal xenotime-(Y), monazite-(Ce) and rutile accompany silicification, carbonatization, potassium matasomatism and chloritization at the Kidd Creek deposit in Canada (Schandl & Gorton 1991).

Quartz veins with REE-U and U-REE±Au mineralization cutting the Early Paleozoic sequences of the Gemeric Superunit show significant increase of U, Au, Cu, Pb, Ca, Y, P, Th, Ag, Co, Sr, La and Mo compared to metamorphosed host black shales (Fig. 23). This enrichment reflects the presence of apatite, xenotime, monazite, uraninite, torbernite, gold, chalcopyrite and pyrite in these veins. The distribution of REE in quartz-apatite veins mostly reflects the presence of dominant xenotime with higher proportion of HREE (Figs. 13, 20, 21). Prevailing LREE in the veins of the Kociha locality may reflect the increased ratio of carbonates in this gangue comparing to other localities. According to experimental data LREE show easier solubility in fluids rich in H_2O and CO_2 (Mysen 1979; Wendlandt & Harrison 1979).

The chemical composition of the non-mineralized Early Paleozoic metamorphosed black sediments (phyllite and lydite) shows a similar association of elements to the above mentioned one in the veins. The contents of Mo, C_{org}, U, Pb, V, Au, Co, Sn, P, Ag, Ca, Y, La and Cu are increased compared to quartz-(chlorite)-sericite phyllite with a low content of organic matter. The distribution of elements in black phyllite and lydite reflects their different lithological control. The C_{org}, Au, P, V, Ag, Sn, U, Mo, Y, Ca, Pb, La and Si contents are higher in lydite than in black phyllite. The increased contents of K, Na, Al, Th, Sr, Ti, Co, Ba, Cu, Cr and B in the black phyllite correspond to the presence of these elements in clastic or clay minerals. Cluster analysis of non-mineralized metamorphosed black sediments of the Gelnica Group also confirms two association of elements. U, Y, La, Au and V show a close correlation to SiO_2, organic carbon and phosphates (CaO and P_2O_5) in lydite (Fig. 24). Th, B, Mo, Sn and Cu on the contrary are bound to Al_2O_3 in black phyllite with detritic quartz and abundant sericite and chlorite. The different behaviour of U and Th is confirmed by the close correlation of Th/Al_2O_3 and U/P_2O_5 (Rojkovič 1997). The distribution of REE also reflects the different origins of the black sediments. The black phyllites representing metamorphosed near-shore clastic sediments show a distribution where LREE are dominant. The ratio of HREE is higher in the lydites representing off-shore sediments (Rojkovič et al. 1995).

The REE-U mineralization in Čučma and Betliar as well as the U-REE±Au mineralization in other localities in the Early Paleozoic sequences of the Gemeric Superunit show an evident spatial and partly also material relationship to the Gemeric Granite. The granite near Čučma shows the highest uranium content of the Western Carpathians granites, with up to 25.4 ppm (Tréger 1972) and 21.0 ppm (Kátlovský 1982).

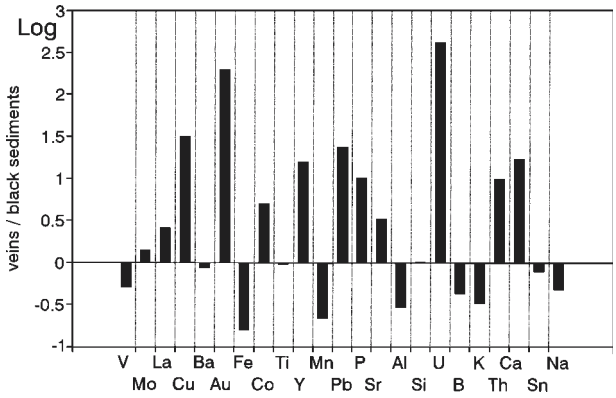

Fig. 23. Enrichment/depletion of elements in veins with REE-U mineralization/metamorphosed black sediments (n = 57 for Fe, Mn, P, Al, Si K, Ca, Na and n = 175 for the other elements).

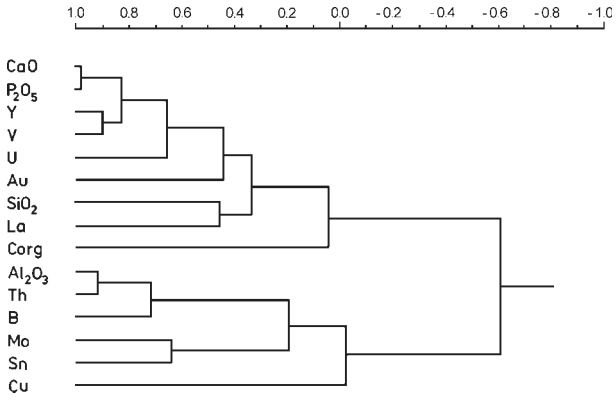

Fig. 24. Cluster analysis of elements in black phyllites and lydites (n = 54, Rojkovič et al. 1995).

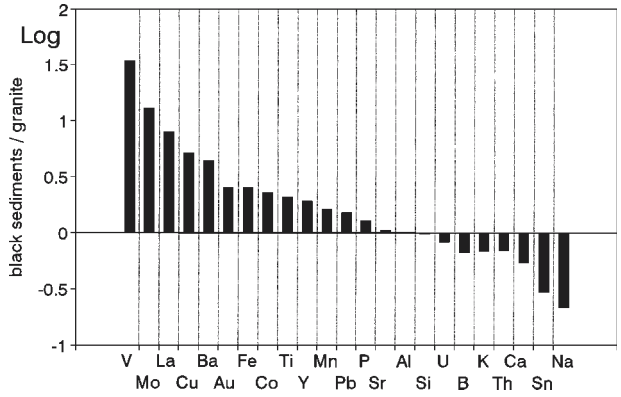

Fig. 25. Enrichment/depletion of elements in metamorphosed black sediments/Gemeric granites (n = 100 for Fe, Mn, P, Al, Si K, Ca, Na and n = 199 for the other elements). Data on non-mineralized rocks outside the mineralized areas by Rojkovič et al. (1995) including data of Vozárová & Ivanička (1993), Cambel & Walzel (1982) and Matula et al. (1983) were calculated.

According to our analyses, the Gemeric Granite is rich in U, Sn, Th and B (Fig. 25). In spite of its large isotopic heterogeneity, Rb-Sr dating of this granite gives, the time of intrusion from 270 to 223 Ma and the younger (Cretaceous) ages correspond to later post-intrusive alteration (Kovách et al. 1986; Cambel et al. 1990). As a reliable U-Pb dating of vein mineralization is missing the Permian age contemporaneous to the Rb-Sr dating of the granite can be taken into account.

Sediments with increased content of organic matter and ore elements are the probable source of the studied mineralization. A similar origin of the U-Au vein mineralization is described from Hoehensteinweg in Germany (Dill 1982). Phosphates associated with metamorphosed black sediments especially lydites with abundant organic matter were a probable source of REE in veins (Rojkovič et al. 1995). During the Hercynian metamorphism siderite-sulphidic veins were formed in the eastern part of the Slovenské rudohorie Mts. by mobilization of Cu, Zn, Ni, Co, Ba, Fe_2O_3 and Sn from black metapelites (Grecula & Radvanec 1988). During the metamorphism and by the hydrothemal activity in proximity to the granite intrusion REE-U vein mineralization was also formed.

The temperature of the studied vein REE-U mineralization is presumed to be 330 to 220 °C according to decrepitation temperatures (Varček 1975). The homogenization temperature of fluid inclusions in quartz associated with U-REE-Au mineralization at Zimná Voda gives T_{hom} from 450 to 300 °C and T_{hom} from 280 to 240 °C for quartz associated with younger sulphides (Kotúlová in Rojkovič et al. 1997). The texture of minerals suggests as a primary association of quartz accompanied by apatite, xenotime and pyrite. During weathering processes REE-bearing minerals of crandallite series (crandallite (?), goyazite and plumbogummite) were formed reflecting a low pH and high content of total dissolved phosphate (Nriagu 1976; Dill et al. 1995). The best bonding to crandallite (?) in Kociha locality shows Ce as was also observed in phosphate mineralization in the Nuba Mountains of Sudan (Dill et al. 1991). Similar zonal variations in the micrometer range of REE contents of authigeneous arsenates of crandallite group have been found in the uranium accumulations in Cenomanian sandstones in the Czech Republic (Scharm et al. 1991). REE-bearing minerals of crandallite series represent secondary products of oxidation accompanied by secondary uranium phosphates (torbernite and autunite) and iron hydroxides.

Conclusions

1) The most important REE mineralization in the Early Paleozoic rocks of the Gemeric Superunit occurs in quartz-apatite veins near the village of Čučma. There are less significant concentrations near Betliar, Helcmanovce and Kociha villages.

2) The REE mineralization is represented by accumulation of xenotime, accompanied by monazite, allanite, goyazite, plumbogummite and crandallite (?) with increased content of LREE. The REE mineralization is accompanied by apatite, uraninite, brannerite, autunite, torbernite, quartz, pyrite, tourmalime, rutile, titanite, marcasite, scheelite and goethite.

3) The contents of REE and Y in range from 0.1 to 0.8 weight percent and rarely exceeds 1 weight percent. The increased proportion of HREE is due to the dominant presence of xenotime.

4) Phosphates associated with metamorphosed black sediments were a probable source of REE in veins. The hydrothermal mineralization was formed by mobilization of ore and REE elements during the metamorphism and by hydrothermal activity in proximity to the Hercynian Gemeric Granite.

Acknowledgements: The study was partly supported by grant VEGA 2/4078/97 and is contribution to IGCP Project No. 373: "Correlation, anatomy and magmatic-hydrothermal evolution of ore-bearing felsic igneous systems in Eurasia". This manuscript benefited greatly by the reviews of Prof. F. Bea, Dr. I. Broska, Dr. I. Petrík and Dr. B. Scharm.

References

Bajaník Š., Ivanička J., Mello J., Reichwalder P., Pristaš J., Snopko L., Vozár J. & Vozárová A., 1984: Geological map of the Slovenské rudohorie Mts., eastern part, 1:50,000. *GÚDŠ,* Bratislava (in Slovak).

Bea F., 1996: Residence of REE, Y, Th and U in granites and crustal protoliths; implications for the chemistry of crustal melts. *J. Petrology,* 37, 521–552.

Beňka J. & Caňo F., 1992: Mineralogy, paragenesis and geochemistry of stibnite veins in the Betliar–Čučma–Volovec area. *Západ. Karpaty, Sér. Mineral. Petrogr. Geochém. Metalogen.,* Bratislava, 15, 61–91 (in Slovak).

Biely A. (Ed.), Bezák V., Elečko M., Kaličiak M., Konečný V., Lexa J., Mello J., Nemčok J., Potfaj M., Rakús M., Vass D., Vozár J. & Vozárová A., 1996: Geological map of Slovakia. *Geological Survey of Slovakia*, Bratislava.

Cambel B. & Walzel E., 1982: Chemical analyses of granitoids of the Western Carpathians. *Geol. Zbor. Geol. Carpath.,* 33, 573–600.

Cambel B., Kráľ J. & Burchart J., 1990: Isotopic geochronology of the Western Carpathian crystalline complex with catalogue of data. *VEDA,* Bratislava, 1–183 (in Slovak with English Summary).

Dill H.G., 1982: Geologie und Mineralogie des Uranvorkommens

am Hoehensteinweg bei Poppenreuth (NE-Bayern) — Ein Lagerstaettenmodell. *Geol. Jahrb*., *(Hannover),* 50, 83.

Dill H.G., Busch K. & Blum N., 1991: Chemistry and origin of vein-like phosphate mineralization, Nuba Mountains (Sudan). *Ore Geol. Rev*., 6, 9–24.

Dill H.G., Fricke A. & Henning K.H., 1995: The origin of Ba- and REE-bearing aluminium-phosphate-sulphate minerals from the Lohrheim kaolinic clay deposit (Rheinisches Schiefergebirge, Germany). *Applied Clay Sci.,* 10, 231–245.

Gbelský J., 1982: Catalogue of accessory minerals of selected samples of granitoid rocks of the Western Carpathians. *Manuscript, GlÚ SAV*, Bratislava, 1–83 (in Slovak).

Grecula P. & Radvanec M., 1988: Mobilization of metals from the Lower Paleozoic black metapelites during metamorphic events (Spišsko-gemerské rudohorie Mts., West Carpathians). In: *Proceedings of the IGCP 254 meeting*, Prague, 29–33.

Kátlovský V., 1982: Die radiometrische Charakteristik Auserwählter Granitoid-Proben der Westkarpaten. *Geol. Zbor. Geol. Carpath*., 33, 729–747.

Kovách A., Svingor E. & Grecula P., 1986: Rb-Sr izotopic ages of granitoids from the Spišsko-Gemerské rudohorie Mts. Western Carpathians. Eastern Slovakia. *Miner. slovaca,* 18, 1–14.

Lottermoser B.G., 1992: Rare earth elements and hydrothermal ore formation processes. *Ore Geol. Rev*., 7, 25–41.

Matula I., Dianiška I. & Radvanec M., 1983. Geochemistry of granites in the Spiško-gemerské rudohorie Mts. *Manuscript*, Bratislava, Geofond (in Slovak).

McLennan S.M. & Taylor S.R., 1979: Rare earth element mobility associated with uranium mineralisation. *Nature*, 282, 247–250.

Melnikova A.M., 1973: Short reports of mineral composition of some uranium occurrences in Slovakia. *Manuscript, URANPRES*, Spišská Nová Ves, 1–88 (in Russian).

Mysen B.O., 1979: Trace elements partitioning between garnet peridotite minerals and water-rich vapor: experimental data from 5 to 30 kbar. *Amer. Mineralogist*, 274–287.

Nriagu J.O., 1976: Phosphate — clay mineral relations in soils and sediments. *Can. J. Earth Sci*., 13, 717–736.

Oberthür T., 1987: Mineralogy and geochemistry of phosphate minerals and brannerite from the proterozoic Carbon Leader Reef gold and uranium placer deposit, Witwatersrand, South Africa. *Monogr. Ser. Miner. Dep.*, *Gebrüder Borntraeger*, Berlin-Stuttgart, 27, 129–142.

Oružinský V., Depta M. & Miškovic J., 1989: Black schists and lydites from the western part of the Gelnica Group, in the contact zone of Gemericum and Veporicum (surroundings of Kociha). In: *Metallogeny and anoxic sediments*, Charles University, Praha, 32.

Pagel M., Pinte G. & Rotach-Toulhoat N., 1987: The rare elements in natural uranium oxides. *Monogr. Ser. Miner. Dep., Gebrüder Bornträger*, Berlin–Stuttgart, 27, 81–85.

Petrík I., Broska I., Lipka J. & Siman P., 1995: Granitoid allanite substitution relations, redox conditions and REE distributions (on an example of I-type granitoids, Western Carpathians, Slovakia). *Geol. Carpathica*, 46, 79–94.

Rojkovič I., 1993: Minerals of the crandallite series in quartz-apatite vein near Čučma. *Miner. slovaca,* 25, 151–153 (in Slovak).

Rojkovič I., 1997: Uranium mineralization in Slovakia. *Acta Geol. Univ. Comen., Monogr. Ser.,* 1–117.

Rojkovič I., Medveď J., Pošta S., Sulovský P. & Walzel E., 1989: Rare earths from uranium mineralization occurrences in the Permian of the Gemericum, the Western Carpathians. *Geol. Zbor. Geol. Carpath*., 40, 453–469.

Rojkovič I., Puškelová Ľ., Khun M. & Medveď J., 1995: U-REE-Au in veins and black shales of the Gemericum, Slovakia. In: Pašava J., Kříbek B. & Žák K. (Eds.): *Mineral deposits*: *from their origin to their environmental impacts. A.A. Balkema*, Rotterdam, Brookfield. 789–792.

Rojkovič I., Háber M. & Novotný L., 1997: U-Au-Co-Bi-REE mineralization in Gemericum, Slovakia. *Geol. Carpathica*, 48, 303–313.

Schandl E.S. & Gorton M.P., 1991: Postore mobilization of rare earth elements at Kidd Creek and other Archean masive sulfide deposits. *Econ. Geol.,* 86, 1546–1553.

Scharm B., Scharmová M., Sulovský P. & Kühn P., 1991: Philipsbornite, arsenflorencite-(La), and arsenflorencite-(Nd) from the uranium district in Northern Bohemia, Czechoslovakia. *Čas. Mineral. Geol.,* Praha, 36, 103–114.

Shmaryovich J.M., Maksimova M.F., Brovin K.G. & Polupanova L.I., 1989: Yttrium and lanthanide behaviour in stratiform – infiltration ore-forming processes. *Litol. Polezn. Iskop*., 6, 39–53 (in Russian).

Šváb J., Tulis J. & Badár J., 1966: Final report about results of geological survey in Čučma locality. *Manuscript, URANPRES,* Spišská Nová Ves, 1–113 (in Slovak).

Tréger M., 1972: Radiochemical characteristic of some Gemeric granites. *Miner. slovaca*, 4, 267–278 (in Slovak).

Tréger M., 1973: Occurrences of uranium–bearing phosphates in the Spišsko-gemerské rudohorie Mts. *Miner. slovaca*, 5, 61–64 (in Slovak).

Varček C., 1975: Mineralogical research of vein uranium mineralization in the central part of the Spišsko-gemerské rudohorie Mts. *Manuscript*, *URANPRES*, Spišská Nová Ves, 1–214 (in Slovak).

Varček C., 1977: Some rare types of mineralization in the Spišsko-gemerské rudohorie Mts. In: *Deposits forming processes in the Western Carpathians. PFUK,* Bratislava, 93–99 (in Slovak).

Varček C., Depta M., Miškovic J. & Oružinský V., 1989: Preliminary results of complex study of anoxic rocks from western part of Gemericum (Paleozoic, Western Carpathians). In: *Metallogeny and anoxic sediments, Charles University*, Praha, 31.

Vocke R.D., Hanson G.N. & Grünenfelder M., 1987: Rare earth element mobility in trhe Roffna Gneiss, Switzerland. *Contr. Mineral. Petrology*, 95, 145–154.

Vozárová A. & Ivanička J., 1993: Lithogeochemistry of Early Paleozoic metasediments in Southern Gemericum. *Západ. Karpaty, Sér. Mineral., Petrogr., Geochém., Metalogen*., 16, 116–149 (in Slovak).

Wendlandt R.F. & Harrison W.J., 1979: Rare earth partitioning between immiscible carbonate and silicate liquids and CO_2 vapor: results and implications for the formation of light rare earth-enriched rocks. *Contr. Mineral. Petrology*, 69, 409–419.